

# Application of Neural Networks for Heart Rate Monitoring

Mohammad Reza Askari\* Iman Hajizadeh\* Mert Sevil\*\*  
Mudassir Rashid\* Nichole Hobbs\*\* Rachel Brandt\*\*  
Xiaoyu Sun\*\* Ali Cinar\*,\*\*

\* *Department of Chemical and Biological Engineering, Illinois Institute of Technology, Chicago, IL 60616 USA*

\*\* *Department of Biomedical Engineering, Illinois Institute of Technology, Chicago, IL 60616 USA*

---

**Abstract:** This paper addresses the problem of heart rate (HR) monitoring from photoplethysmography (PPG) sensors, where artifacts caused by body movements drastically affect the quality of the measurement signal. The PPG signal is windowed into consecutive segments, and for each time-windows, a Butterworth bandpass filter is utilized to attenuate high-frequency noises. Then, the PPG signal is processed by using the singular spectrum analysis technique to obtain a smooth PPG signal. In order to remove artifacts caused by the physical activity of the subject, the 3-dimensional accelerometer signal is used as an auxiliary signal to detect the presence of motion artifact (MA). A new spectral subtraction approach is proposed for MA rejection. For the purpose of HR estimation from the PPG signal, a feature extraction method is performed, and neural network binary classifier is used to detect the most probable frequencies corresponding to the actual HR. HR estimations are passed through a Kalman filter to result in smooth and accurate HR estimations.

*Keywords:* Developments in measurement, Filtering and smoothing, Heart rate estimation, Neural networks, Signal processing.

---

## 1. INTRODUCTION

Artifacts are disturbances in the measured signal not originating from the process itself, and due to intense corruption of the photoplethysmography (PPG) signal, artifact removal necessitates further investigation. One application where artifacts are prevalent is the estimation of heart rate (HR) using the PPG signal. PPG is an optical technology, which is widely used in wristbands and sports watches to provide an inexpensive and noninvasive method for HR estimation. The main drawback of the PPG signal is that the approach is highly susceptible to corruption from motion artifacts (MA) caused by movement. Besides, ambient light disrupts the functionality of the sensor (Zhang et al. (2015b)), which makes the PPG-based method less accurate than the electrocardiogram (ECG) recordings. Artifact removal from a noisy signal is a challenging task because artifacts in the signals are caused by several unknown sources. Furthermore, discriminating between MA and the actual variation of the HR in the PPG signal is a challenging issue because of their similar behavior and having overlapping frequencies in their periodogram. General sources of measurement error include ambient light interference, the location of LED sensors at

which the signal being recorded, skin pigmentation, and poor contact between the measurement skin surface and the photo-sensor (Castaneda et al. (2018); Zhang et al. (2015a); Zhang et al. (2015b)).

A PPG cleaning and MA removal algorithm is developed to generate robust and reliable estimates of the HR by using similarity-based spectral subtraction-signal processing. The estimate of HR is obtained by using the Fast Fourier Transform (FFT) and solving a binary classification problem. Kalman filtering (KF) is used to provide a smooth and accurate estimate of HR. The results show the effectiveness of the proposed denoising and estimation method.

### 1.1 Related Works

Several algorithms are proposed to address the problem of PPG signal denoising in the presence of MA disruptions. A framework to remove the disturbance of motion artifact in the spectrogram of the PPG signal is proposed by Zhang et al. (2015b), which employs singular value decomposition (SVD) to cancel the MA and high-frequency noises. To further enhance the robustness of the scheme, temporal difference operation is applied, and in the final step of signal denoising, spectral signal reconstruction is utilized to approximate the PPG signal with the sparsest signal. Finally, the spectrogram of the PPG signal is calculated by FFT to estimate HR values. Another approach uses the ensemble empirical mode decomposition (EEMD) denoising technique to remove MA proposed by Khan et al.

---

\* Financial support from the National Institutes of Health (NIH) under the grants 1DP3DK101075 and 1DP3DK101077 and Juvenile Diabetes Research Foundation (JDRF) grant 2-SRA-2017-506-M-B made possible through collaboration between the JDRF and The Leona M. and Harry B. Helmsley Charitable Trust is gratefully acknowledged.

(2016). When EEMD fails to denoise the signal, three steps of adaptive nonlinear recursive least squares (NRLS) filtering are performed to reduce the effects of unwanted oscillations in the PPG signal caused by the MA. An adaptive recursive least squares filtering accompanied by a binary decision making step is suggested to decrease the MA in the observed PPG signal (Ye et al. (2016)). The Pearson correlation coefficient between filtered PPG signal and 3-dimensional accelerometer signal is used to identify further the MA associated with PPG signal. The sparse signal reconstruction technique is proposed to estimate the spectrogram of the PPG signal and detect the location of the peak corresponding to the HR (Zhang et al. (2015c)). An efficient approach to threshold eigenvalues in SVD signal refining method is also proposed by Galli et al. (2018), and the HR estimation is performed using the spectrogram of the PPG signal (Zhang et al. (2015a); Temko (2015)). Using Kalman filtering (KF) demonstrates a significant improvement in smoothing the reported values for HR estimation. In another work, kurtosis and skewness classification is employed to determine the best method from one of FFT, SVD, or independent component analysis to synthesize the reference signal for adaptive step-size least mean squares filter (Ram et al. (2012)).

### 1.2 Contributions

In this work, an efficient approach is proposed to remove MA disturbances in the PPG signal and estimate the HR values from the refined signal. The frequency of MA and noise are estimated from the power spectrum of the 3-dimensional accelerometer signal and subtracted from the artifact-corrupted PPG signal to reconstruct the power spectrum of the rectified PPG signal. The HR values are estimated using well-known zero-padded FFT techniques and Neural Network (NN) binary classifier. A single random walk model and KF are utilized to enhance the accuracy of the HR estimation by smoothing the estimated HR values. The results and classification performance indexes confirm the effectiveness of the proposed signal denoising, HR estimation, and motion artifact recognition scheme.

- A novel similarity-based spectral subtraction signal processing technique is proposed to separate disrupting motion artifact from the PPG signal. The proposed technique is capable of attenuating the magnitude of the frequency corresponding to MA and amplifying that of the HR.
- An NN classifier is used to model the trajectory of heartbeats from the power spectrogram of the PPG signal in each time-windows. The proposed model is robust enough to prevent inaccurate and misleading HR estimation from the signal.
- The algorithm is computationally efficient, suitable for real-time implementation in wearable sensors for HR monitoring or other clinical purposes such as measuring blood oxygen saturation.

The remainder of this paper is organized as follows: The proposed method, including the proposed MA removal technique and the HR estimation method used in this study, are briefly presented in section 2. Section 3 explains the dataset used in this study and also presents simulation

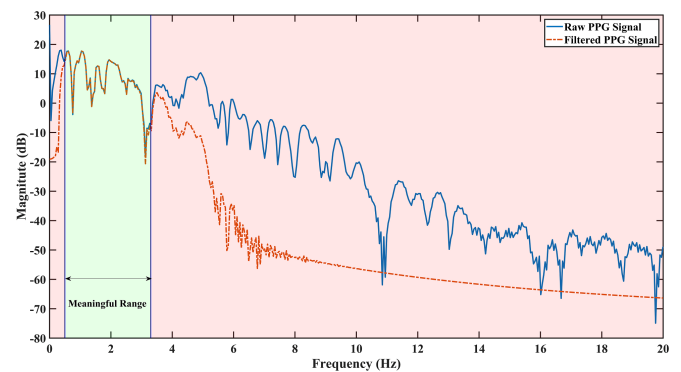


Fig. 1. The power spectrum of the unprocessed PPG signal (solid blue line) and bandpass filtered PPG signal (dashed-dotted red line).

results for the proposed method. section 4 gives some concluding remarks.

## 2. PROPOSED METHOD

HR estimation from the PPG signal consists of four main steps: Pre-Processing, Signal Processing, Peak Tracking and HR estimation, and Post-Processing and Smoothing. The different steps of the technique are described briefly.

### 2.1 Pre-processing

The first step of motion artifact removal and HR estimation is time-windowing, in which the online measurement PPG and triple-axis accelerometer signals are broken into consecutive time windows. Batch wise processing of signals provides us the benefit of using the information from the past windows; therefore, more consistent and realistic HR estimation is obtained. A time-window of  $T_s$  seconds and the sliding time of  $S$  seconds is considered such that  $S \leq T_s/2$ . More overlapping time-windows improve the accuracy of HR estimation and MA removal; however, it enhances the computational effort for processing and heartbeat estimation and tracking. Depending on the frequency of signal sampling, the available power of computation, and the accuracy of estimation, the size of the time-window and the sliding time is determined. For the set of data used in this study, a time-window of 8 seconds and a sliding time of 2 seconds, resulting in 75% overlap between consecutive windows, are chosen. The PPG signal and triple-axis accelerometer data are corrupted by a broad range of relatively high frequency and low magnitude noises. Therefore, the rejection of noises such that the filtered PPG signal represents the meaningful information of the heart activity is a crucial task. Regardless of the various known and unknown factors affecting the HR, a range of [30, 220] beats per minute (BPM) with the corresponding frequency of [0.5, 3.7] Hz is considered as a proper range encompassing all possible realizable values of the HR. The PPG and acceleration signals are normalized to a value between  $[-1, 1]$  and passed through 6<sup>th</sup> order Butterworth bandpass filter to reject all noises outside of the desired interval. Fig. 1 demonstrates the difference in the power spectrum of stop-bands in decibels for the bandpass filter used in this study.

## 2.2 Signal Processing

The frequency band of motion artifact range from 0.1 Hz to 20 Hz, which overlaps all possible frequencies of the HR values (Shimazaki et al. (2014)), and consequently, the artifact-corrupted PPG signal impedes the discrimination between desired PPG and MA. Singular spectrum analysis (SSA) of the time-series data is a widely utilized technique for separating high-frequency ripples. Let the lagged L-trajectory matrix  $Y \in R^{L \times J}$  of the time-series PPG signal,  $y \in R^N$ , is approximated with  $D < \min\{L, J\}$  components as expressed by Eq. (1) as

$$Y_{L \times J} \approx \sum_{j=1}^D Y_i \quad (1)$$

where  $Y_i$  are rank-one decomposed trajectory matrices. Performing SSA requires four steps: 1. trajectory matrix embedding, 2. singular value decomposition, 3. matrix grouping, and 4. signal reconstruction (Maddirala and Shaik (2016)). In the trajectory matrix embedding, the Hankel matrix  $Y$  is constructed from each segment of the windowed times series PPG signal  $y = [y_1, \dots, y_N]$  as:

$$Y \triangleq \begin{bmatrix} y_1 & y_2 & \dots & y_J \\ y_2 & y_3 & \dots & y_{J+1} \\ \vdots & \vdots & \ddots & \vdots \\ y_L & y_{L+1} & \dots & y_N \end{bmatrix}_{L \times J}$$

As suggested, to obtain a proper resolution in decomposition, based on the sampling frequency  $f$  and the frequency of the desired signal, constants  $L$  and  $J$  are chosen in such a way that  $L > f_f/f_d$  and  $N = L + J - 1$  Teixeira et al. (2006); James and Lowe (2003). In the SVD step, rank-one trajectory matrices  $Y_1, \dots, Y_L$  are calculated from the eigen matrices. Lets denote scalars  $\lambda_1 \geq \lambda_2 \geq \dots \geq \lambda_L$  eigen values of the the positive semi definite matrix  $Q = Y \times Y^T$ . Then, the trajectory matrices,  $Y_i$ , are calculated as:

$$Y_i = \sqrt{\lambda_i} U_i V_i^T, i = 1, \dots, L \quad (2)$$

where  $U_i$  and  $V_i$  are the left and right triangular vectors corresponding to eigenvalues  $\lambda_i$ , respectively. The Henkel trajectory matrix  $Y$  is obtained by adding  $Y_i$  up to  $i = L$ . However, for the signal processing and noise reduction purposes, only trajectory matrices  $Y_i$  corresponding to the actual signal are summed to obtain the approximation of the Henkel matrix as:

$$\hat{Y} = \sum_{k_i \notin K_{noise}} Y_{k_i} \quad (3)$$

where  $K_{noise} \triangleq \{k_1, \dots, k_D\} (D < L)$  is the set containing indices of eigenvalues corresponding to the noise. In the last step of SSA, the estimation of the time series PPG signal  $\hat{y} = [\hat{y}_1, \dots, \hat{y}_N]$  is obtained by adding up diagonal-averaged vectors calculated from the trajectory matrix  $Y_{k_i}$  Golyandina et al. (2001). By using band-pass filtering and SSA, meaningless noises and high-frequency ripples in the power spectrum of the PPG signal are eliminated. However, the main issue, which is the existence of MA, causes a significant obstacle toward HR estimation. To further analyze the behavior of the PPG signal corrupted with MA, FFT has been widely utilized by many researchers to

establish the frequency representation of the PPG signal as

$$\hat{y}_{r,k} = \sum_{n=0}^{N-1} \hat{y}_{r,n} e^{-\frac{2\pi k n i}{N_z}}, k = n_{lf}, \dots, n_{hf} \quad (4)$$

where  $\hat{y}_{r,k} \in R^{(n_{hf}-n_{lf}+1)}$  are the frequency bins of the estimated PPG,  $\hat{y}_{r,n}$  and  $n_{lf}$  and  $n_{hf}$  represent the indices of the frequency bins corresponding to the minimum and maximum possible HR values, respectively. To have a better resolution of the power spectrum, zero-padded PPG signal,  $\hat{y}_r \in N_z$ , is used instead of the vector of the PPG signal itself. For simplicity in HR calculation,  $N_z - N$  interpolation points are added to the vector of the PPG signal, which each frequency bin  $\frac{60 \times f_s}{N_z}$  corresponds to 1 BPM. Therefore, the augmented vector of the PPG signal is utilized to calculate spectral bins:

$$\hat{y}_r = \underbrace{[\hat{y}_1, \hat{y}_2, \dots, \hat{y}_N]}_{\text{PPG vector}} \underbrace{[0, 0, \dots, 0]}_{\text{zero-padded elements}} \quad (5)$$

where  $N_z = 60 \times f_s$ . Spectral bins calculated by (4) and (5) not only reduce the computational burden caused by calculating the magnitude of only necessary frequencies but also enhance the accuracy of the power spectrum of the PPG signal by using more interpolation points. Lets  $N_{\hat{y}_{r,k}} = \|\hat{y}_{r,k}\|$  and  $N_{\hat{y}_r} = [N_{\hat{y}_{r,1}}, \dots, N_{\hat{y}_{r,(n_{hf}+n_{lf}+1)}}]$ . As mentioned in Askari et al. (2020), the 3-dimensional accelerometer signal is a proper reference for detecting MA and obviously, the existence of MA can be observed in the power spectrum of both PPG and accelerometer signals. In order to separate the magnitude of frequencies corresponding to MA from the power spectrum of PPG signal, it is desired to minimize the *Cos* similarity between the power spectrum of two signals as:

$$\cos(\theta) = \frac{N_{\hat{y}_r} \cdot N_{a_t}}{\|N_{\hat{y}_r}\| \|N_{a_t}\|}, a_t \in \{a_x, a_y, a_z\} \quad (6)$$

where  $a_t$  denote the accelerometer signal in direction  $t$  and  $N_{a_t} \in R^{(n_{hf}+n_{lf}+1)}$  stand for the vector of power spectral bins of the 3-dimensional accelerometer signals. To obtain the minimum *cos* similarity between each pair of PPG and accelerometer signal, the orthogonal power spectrum of the PPG signal can be achieved through Eq.(7)

$$N_{\hat{y}_r \perp a_t} = N_{\hat{y}_r} \left( I_{(n_{hf}-n_{lf}+1)} - \frac{N_{a_x, y, z} N_{a_x, y, z}^T}{N_{a_x, y, z}^T N_{a_x, y, z}} \right) \quad (7)$$

where  $N_{a_x, y, z} = [N_{a_x}, N_{a_y}, N_{a_z}] \in R^{(n_{hf}+n_{lf}+1) \times 3}$ . The reconstructed power spectrum  $N_{\hat{y}_r \perp a_t}$  has the maximum angular distance from each accelerometer signal, which means the power spectrum of frequencies corresponding to the actual HR is magnified, and the magnitude of other frequencies are attenuated. Some reconstructed spectral bins take negative values which are normalized as

$$N_{\hat{y}_r \perp a_x, y, z, k} = \begin{cases} 0, & N_{\hat{y}_r \perp a_x, y, z, k} \leq 0 \\ \frac{N_{\hat{y}_r \perp a_x, y, z, k}}{\max(N_{\hat{y}_r \perp a_x, y, z})}, & N_{\hat{y}_r \perp a_x, y, z, k} > 0 \end{cases} \quad (8)$$

The location of the most dominant peaks corresponding to the HR before and after similarity-based spectral subtraction are displayed in Fig. 2.

### 2.3 Peak Tracking and Heart Rate Estimation

Theoretically, the most dominant peak in the power spectrum of the PPG signal is the representative of the actual HR. However, all peaks in the power spectrum have different probabilities of being recognized as the real HR peaks. In a simple way, we can choose the most dominant peak as the actual HR peak in the power spectrum of the PPG signal. However, we are ignoring the fact that HR estimated in two consecutive time-windows are close in their values. This statement can be justified by the fact that there is 75 % overlap between consecutive time-windows, and the power spectrum of each time-window of the PPG signal is similar to that of the previous one. As a consequence, the difference between the actual HR in each time-window and the actual heart rate observed in the previous time window rarely exceeds 7 BPM (Zhang et al. (2015b)). Additionally, narrow peaks in the power spectrum are more interesting for consideration in comparison to wide-basis peaks because they represent more harmonic HR waves in the spectrum of the PPG signal. In this regard, it is desired to find a model to check the possibility of every candidate peak for being the actual HR peak in each time-window of the PPG signal. In order to find the most probable peak in each time-window of the PPG signal, an NN classifier is utilized to check each peak in the power spectrum of the PPG signal. The magnitude of each peak, the difference in location of the peak with the actual HR peak in the previous time window, and the width of each peak are considered as the input of the classifier. Fig. 3 depicts the three features used for binary classification.

Since HR estimation using this algorithm requires calculating features based on the previous time-windows, initialization for the first time-window is required. Furthermore, there is no prior information about the potential range of the actual HR, and many other peaks can be interpreted as real heartbeat by mistake, for the first time window, the

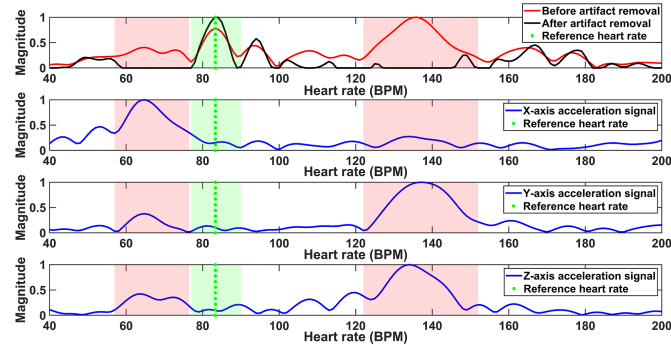


Fig. 2. An example showing the effectiveness of the similarity-based spectral subtraction algorithm. The spectrum of the PPG signal before spectral subtraction (solid red line), the PPG signal after spectral subtraction (solid black line), ground-truth of the HR value (green bullets), spectral bins affected by MA (red shaded region), and spectral bins representing the frequency of HR (green shaded region), and (b) the spectrum of the acceleration signal in the x-axis (solid blue line), (c) the spectrum of the acceleration signal in the y-axis (solid blue line), and (d) the spectrum of the acceleration signal in the z-axis (solid blue line).

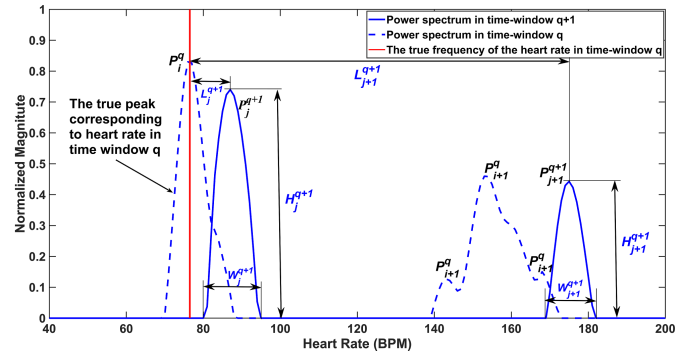


Fig. 3. The power spectrum of the PPG in the previous time-window (dashed blue line), the power spectrum of the PPG signal in the present time-window (solid blue line), and the location of the actual HR in the previous time-window (solid red line).  $H_j^{q+1}$ ,  $W_j^{q+1}$ , and  $L_j^{q+1}$  are three utilized features for binary classification and are defined as height, width, and difference between  $j^{th}$  peak in  $q^{th}$  time-windows.

subject is asked to keep the recording device motionless as much as possible for several seconds to obtain a clean PPG recording. Then, instead of estimating HR from the NN classifier in the first time-window, we choose the frequency of the most dominant peak in the spectrogram of the PPG signal as the HR value. Calculating the feature variables of the next time-windows is feasible by using the location of the most portable candidate peak in the previous time-window.

The structure of the NN used for HR peak detection consists of an input layer to feed three vectors of the features; a long-short-term-memory (LSTM) to take into account time-series variation of the HR, and also the fact that the location, magnitude, and the width of actual HR peaks obey a time-series type of variation; a fully connected layer with rectified linear unit (RELU) activation function, and a softmax layer with two outputs. The sketch of the NN classifier used in this study is demonstrated via Fig. 4.

### 2.4 Postprocessing and Smoothing

The estimated HR from the previous step is a raw estimation due to nonsmooth oscillatory behavior. Although most oscillations and extreme variations of the estimated HR can be addressed in the smoothing step, the raw measurement does not have the accuracy of a smooth HR estimation. To further increase the accuracy of the

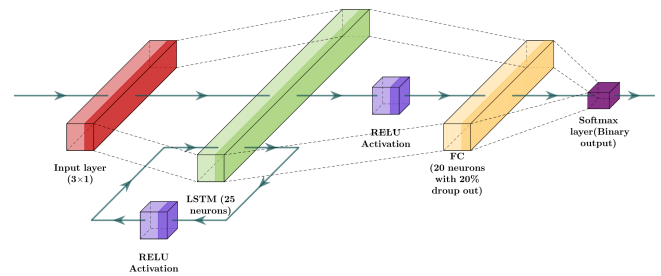


Fig. 4. The sketch of the NN classifier for binary classification problem.

estimation, a discrete-time random walk dynamic system is employed to model the variation of the HR in each successive time-window as

$$\begin{cases} \theta(k) = \theta(k-1) + \omega(k) \\ z(k) = \theta(k) + \nu(k) \end{cases} \quad (9)$$

where  $\theta(k)$  and  $z(k)$  are the raw estimate of the HR in the current time-window and the measurement variable incorporating the uncertainty, respectively.  $\omega(k)$  and  $\nu(k)$  denote zero-mean random variables with standard deviation  $\sigma_\omega$  and  $\sigma_\nu$  representing the uncertainty in the dynamics and the measurements of the actual HR, respectively (Galli et al. (2018)). The standard deviation of the measurement noise can be determined from prior knowledge on the discrepancy between the actual and estimated values for the HR. Similarly, the process noise is estimated from historical knowledge on the variation of HR between two consecutive time-windows. The processed estimation of the HR is calculated from the following KF given by Eq. (10) for HR smoothing.

$$\begin{cases} \hat{\theta}(k+1) = \hat{\theta}(k) + \frac{p(k)e(k-1)}{p(k) + \sigma_\nu^2} \\ e(k) = z(k) - \hat{\theta}(k) \\ p(k+1) = \frac{p(k)}{p(k) + \sigma_\nu^2} \sigma_\omega^2 + \sigma_\omega^2 \end{cases} \quad (10)$$

where  $\hat{\theta}(k)$  represents the smoothed estimation of the HR, and  $p(k)$  stand for the state prediction variance.

### 3. SIMULATION RESULTS AND DISCUSSION

A set of open access experimental datasets as a part of the IEEE Signal Processing Cup 2015 is used in this work (Zhang et al. (2015b)). Twelve selected subjects are aged from 18 to 35, and the procedure of 5 minutes treadmill experiment includes a half minute in resting condition (1-2 km/h), one minute of walking (6-8 km/h), one minute of running (12-15 km/h), another minute of walking and running, and the last half-minute resting, respectively. Two channels of PPG signal are recorded via an electronic wristband device with a green light-emitting diode, producing the wavelength of 515 nm, a triple-axis acceleration signal, and one channel of ECG signal. All quantities are measured at 125 Hz sampling rate. The corresponding reference values of the HR are extracted from the ECG

Table 1. The value of adjustable parameters used in the NN classifier model.

Variable	Value/Technique
Number of connection in the fully connected layer	25
Number of connection in the LSTM layer	20
Learning rate	$10^{-3}$
Optimization algorithm	Adam
Gradient decay factor	0.1
Size of batches	1000
L2 regularization factor	$10^{-2}$
Momentum factor	0.92
Activation function	RELU
Validation check	every 50 epoches

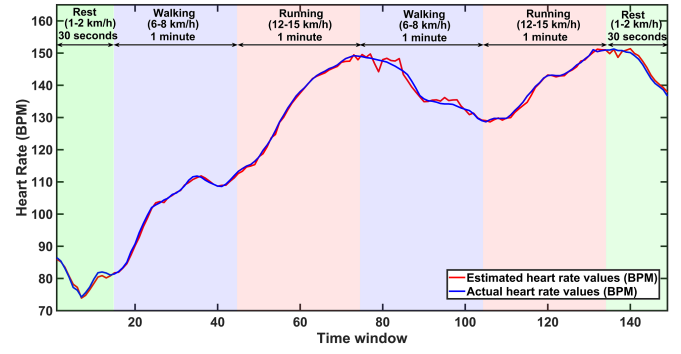


Fig. 5. The trajectory of the actual HR (solid blue line) and smoothed estimation of the HR (solid red line) for subject 5.

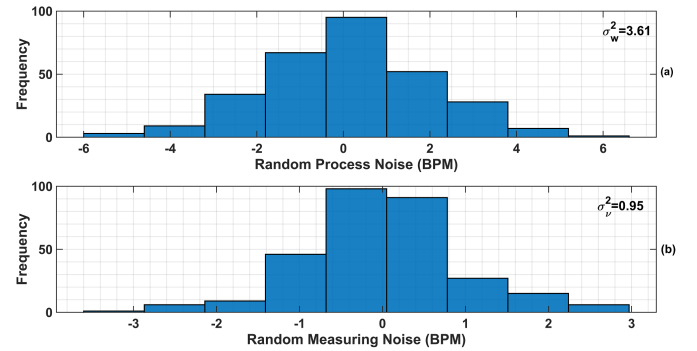


Fig. 6. (a) Deviation of estimated HR for two consecutive time-windows (random process noise) and (b) deviation of the estimated HR from their actual values calculated from the ECG signal (random measurement noise).

signal recorded by electrode sensors attached to the chest strap device. In order to examine the effectiveness of the proposed method, the algorithm is tested with all twelve datasets. For each simulation study, nine datasets are chosen randomly for the training and validation of the NN classifier. One dataset is used to evaluate the performance of the algorithm. In order to obtain a more realistic estimation, two randomly chosen datasets are used to calculate the variance of process and measurement noises appeared in Eq. (9). The adjustable parameters of the NN classifier are shown in the Table. 1.

Fig. 5 demonstrates the estimated HR values during five minutes treadmill experiment for a randomly chosen subject (subject 5). Two remained datasets, including 315 sample points, are chosen to plot the histogram and calculate the variance of the process and measurement noise as shown in Fig. 6. In order to enhance the accuracy of estimation, as shown in Fig. 5, the variances of the random process noise,  $\sigma_w^2$ , and the random measurement noise,  $\sigma_\nu^2$ , are calculated as 3.61 and 0.95, respectively from two histograms shown by Fig. 6. The estimated HR values are smoothed and to further enhance the HR estimation of Fig. 5

The binary classification results, including the accuracy and F1 score for all twelve subjects are summarized in Table 2. The number of correctly predicted HR peaks (TP), correctly predicted noise and artifact peaks (TN),

Table 2. Binary classification results for all subjects.

Subj	Accuracy (%)	F1 Score (%)	no. TP	no. TN	no. FP	no. FN
1	95.82	74.00	121	1831	65	20
2	98.08	86.84	132	1920	29	11
3	99.74	98.20	137	1841	3	2
4	99.34	95.20	139	1980	11	3
5	99.77	98.28	143	2088	3	2
6	98.82	91.80	140	1958	16	9
7	99.20	94.11	136	1972	11	6
8	99.9	99.36	157	2147	1	1
9	99.82	98.65	147	2141	3	1
10	95.64	70.48	109	2052	92	35
11	99.95	99.65	142	2057	1	0
12	98.31	88.27	143	2075	34	4

wrongly predicted artifacts as noise (FP), and wrongly predicted HR peaks as artifacts (FN) are provided in the table. Overall, 22176 noisy and corrupted peaks and 1608 HR-related peaks in all power spectrums are observed, and 99.2% of all corrupted peaks and 95.8% of actual HR peaks are correctly classified. From high accuracy and F1 score provided Table 2 for all subjects, one can realize that the effect of MA in the spectrum of the PPG signal is significantly eliminated.

#### 4. CONCLUSION

This paper addresses the problem of noise and MA reduction from the wristband PPG signal during intense physical activity and develops an algorithm to estimate HR from the processed signal. The spectrum of the MA is estimated from 3-dimensional accelerometer signals, and FFT is used to calculate only meaningful frequencies of the refined PPG signal to decrease the computational burden. Unlike adaptive filters used by many researchers for artifact removal, a novel similarity-based spectral subtraction technique is suggested to reject MA. A binary NN classifier is utilized to estimate the HR from the spectrum of the PPG signal. For each simulation study, two random datasets are used to calculate the variance of the random process noise and random measuring noise, and KF is employed to smooth the HR estimates. The trajectory of the estimated HR and binary classification results demonstrate the effectiveness of the proposed approach. The developed algorithm is computationally efficient and suitable for real-time implementation as only the spectrum of a narrow frequency-range of the PPG signal is processed. Besides, the Neural Network model needs to be trained and personalized only once in order to be used for real time hear rate estimation.

#### REFERENCES

Askari, M.R., Rashid, M., Sevil, M., Hajizadeh, I., Brandt, R., Samadi, S., and Cinar, A. (2020). Artifact removal from data generated by nonlinear systems: Heart rate estimation from blood volume pulse signal. *Industrial & Engineering Chemistry Research*, 59(6), 2318–2327.

Castaneda, D., Esparza, A., Ghamari, M., Soltanpur, C., and Nazeran, H. (2018). A review on wearable photoplethysmography sensors and their potential future applications in health care. *International journal of biosensors & bioelectronics*, 4(4), 195.

Galli, A., Narduzzi, C., and Giorgi, G. (2018). Measuring heart rate during physical exercise by subspace decomposition and kalman smoothing. *IEEE Transactions on Instrumentation and Measurement*, 67(5), 1102–1110.

Golyandina, N., Nekrutkin, V., and Zhigljavsky, A.A. (2001). *Analysis of time series structure: SSA and related techniques*. Chapman and Hall/CRC.

James, C.J. and Lowe, D. (2003). Extracting multisource brain activity from a single electromagnetic channel. *Artificial Intelligence in Medicine*, 28(1), 89–104.

Khan, E., Al Hossain, F., Uddin, S.Z., Alam, S.K., and Hasan, M.K. (2016). A robust heart rate monitoring scheme using photoplethysmographic signals corrupted by intense motion artifacts. *IEEE Transactions on Biomedical Engineering*, 63(3), 550–562.

Maddirala, A.K. and Shaik, R.A. (2016). Removal of eog artifacts from single channel eeg signals using combined singular spectrum analysis and adaptive noise canceler. *IEEE Sensors Journal*, 16(23), 8279–8287.

Ram, M.R., Madhav, K.V., Krishna, E.H., Komalla, N.R., and Reddy, K.A. (2012). A novel approach for motion artifact reduction in ppg signals based on as-lms adaptive filter. *IEEE Transactions on Instrumentation and Measurement*, 61(5), 1445–1457.

Shimazaki, T., Hara, S., Okuhata, H., Nakamura, H., and Kawabata, T. (2014). Cancellation of motion artifact induced by exercise for ppg-based heart rate sensing. In *2014 36th Annual International Conference of the IEEE Engineering in Medicine and Biology Society*, 3216–3219. IEEE.

Teixeira, A.R., Tomé, A.M., Lang, E.W., Gruber, P., and Da Silva, A.M. (2006). Automatic removal of high-amplitude artefacts from single-channel electroencephalograms. *Computer methods and programs in biomedicine*, 83(2), 125–138.

Temko, A. (2015). Estimation of heart rate from photoplethysmography during physical exercise using wiener filtering and the phase vocoder. In *Engineering in Medicine and Biology Society (EMBC), 2015 37th Annual International Conference of the IEEE*, 1500–1503. IEEE.

Ye, Y., Cheng, Y., He, W., Hou, M., and Zhang, Z. (2016). Combining nonlinear adaptive filtering and signal decomposition for motion artifact removal in wearable photoplethysmography. *IEEE Sensors Journal*, 16(19), 7133–7141.

Zhang, Y., Liu, B., and Zhang, Z. (2015a). Combining ensemble empirical mode decomposition with spectrum subtraction technique for heart rate monitoring using wrist-type photoplethysmography. *Biomedical Signal Processing and Control*, 21, 119–125.

Zhang, Z., Pi, Z., and Liu, B. (2015b). Troika: A general framework for heart rate monitoring using wrist-type photoplethysmographic signals during intensive physical exercise. *IEEE Transactions on biomedical engineering*, 62(2), 522–531.

Zhang, Z. et al. (2015c). Photoplethysmography-based heart rate monitoring in physical activities via joint sparse spectrum reconstruction. *IEEE Trans. Biomed. Engineering*, 62(8), 1902–1910.